THE JOURNAL OF PHYSICAL CHEMISTRY B

Article

pubs.acs.org/JPCB

New Insights on the Molecular Recognition of Imidacloprid with *Aplysia californica* AChBP: A Computational Study

José P. Cerón-Carrasco,*[,†] Denis Jacquemin,[†,‡] Jérôme Graton,[†] Steeve Thany,[§] and Jean-Yves Le Questel*[,†]

[†]Université de Nantes, UMR CNRS 6230, Chimie Et Interdisciplinarité: Synthèse, Analyse, Modélisation (CEISAM), UFR Sciences & Techniques, 2, rue de la Houssinière, BP 92208, 44322 NANTES Cedex 3, France

[‡]Institut Universitaire de France, 103, bd Saint-Michel, F-75005 Paris Cedex 05, France

[§]Université d'Angers, Récepteurs et Canaux Ioniques Membranaires, UPRES EA 2647, USC INRA 2023, UFR Sciences, 2 boulevard Lavoisier, 49045 Angers Cedex, France

Supporting Information

ABSTRACT: The binding of imidacloprid (IMI), the forerunner of neonicotinoid insecticides, with the acetylcholine binding protein (AChBP) from *Aplysia californica*, the established model for the extracellular domain of insects nicotinic acetylcholine receptors, has been studied with a two-layer ONIOM partition approach (M06-2X/6-311G(d):PM6). Our calculations allow delineating the contributions of the key residues of AChBP for IMI binding. In particular, the importance of Trp147 and Cys190−191, through weak CH···π interactions and both van der Waals and hydrogen-bond (H-bond) interactions, respectively, are highlighted. Furthermore, H-bonds between hydroxyl groups of both Ser189 and Tyr55 and the IMI nitro group are pointed out. The participation of Ile118, whose main chain NH and carbonyl group are hydrogen-bonded with the IMI pyridinic nitrogen through a water molecule, is characterized. Our simulations also indicate the presence of a significant contribution of this residue through van der Waals interactions. The various trends obtained by the calculations of the pairwise interaction energies are confirmed through a complementary noncovalent interaction (NCI) analysis of selected IMI−AChBP amino acid pairs. Indeed, the contribution of a halogen-bond interaction between IMI and AChBP, recently proposed in the literature, is corroborated by our NCI analysis.

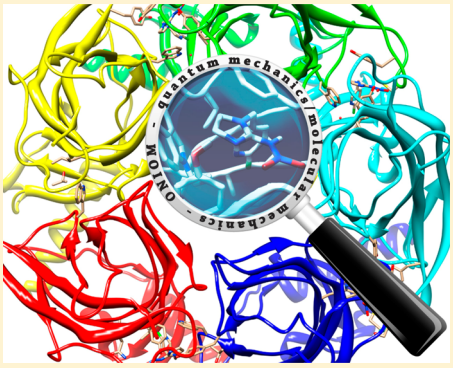

1. INTRODUCTION

Nicotinic acetylcholine receptors (nAChRs) are members of the Cys-loop ligand-gated ion channels (LGICs) superfamily, which also includes GABA, glycine, and 5-HT3 receptors.[1−3] These neuroreceptors play a pivotal role in the synaptic transmission inside vertebrate and insect nervous systems, since they receive and analyze the chemical signals between neurons in the nervous system and convert them into an electrical output. In these pentameric LGICs, the five subunits are symmetrically or pseudosymmetrically arranged around a central ion-conducting pore, forming homo- or heteropentamers of related subunits.[1−3] The nAChRs are therefore important targets for the design of human and veterinary drugs as well as insecticides. However, the functional organization of nAChRs, as well as their diversity in terms of subunit composition and stoichiometries, is much better known in vertebrates than in insects.[4−6]

Among the various classes of insecticides, neonicotinoid is considered as the most important and the fastest growing one. Indeed, neonicotinoids are currently used in more than 120 countries and are particularly effective insecticides for controlling sucking insects.[7,8] Imidacloprid (IMI) (Figure 1), the forerunner of this class, composed of chloropyridinylmethyl and *N*-nitroimine moieties, remains the key representative of these compounds.[9] The nature of neonicotinoid−nAChR interactions has been partially analyzed through both chemical and structural biology investigations as well as through molecular biology approaches such as site-directed mutagenesis or chimeragenesis.[10−13] However, the future of neonicotinoids is bound to two important issues: (1) the development of

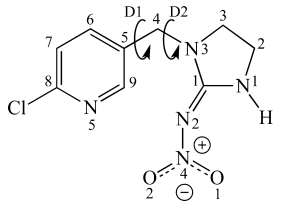

Figure 1. Chemical structure and atomic numbering of IMI. The D1 and D2 dihedral angles used in the exploration of the potential energy surface are displayed.

Received: October 16, 2012
Revised: March 21, 2013
Published: March 22, 2013

resistance in pests and (2) the adverse effects on beneficial insect species such as honey bees.

The understanding of the neonicotinoid−nAChR binding mode has been greatly facilitated by the discovery and crystallization of soluble ACh binding proteins (AChBPs) from the saltwater mollusk *Aplysia californica* (*Ac*) and the freshwater snail *Lymnaea stagnalis* (*Ls*), which are established models for the extracellular ligand-binding domain (LBD) of the nAChRs.[14−16] From these crystal structures, a common conception for the nAChR LBD−neonicotinoid interactions has been derived, which clearly differs from the binding modes of nicotinoids. The IMI binding mode, revealed in 2008 by crystallography, agrees with previous photoaffinity-labeling results.[15,16] Two IMI−AChBP complexes have been almost simultaneously resolved through X-ray diffraction with respective resolutions of 2.58 and 2.48 Å, using AChBPs of *Ac* and *Ls* species.[15,16] Among these structures, only *Ac*−AChBP (PDB code 3C79) has been shown to be pharmacology reminiscent for the insect nAChR subtypes, that is, to present high neonicotinoid sensitivity, and consequently, it has been selected as the PDB entry in the present work. This structural biology analysis reveals: (i) orientations of functional amino acids in the ligand-bound state, (ii) conformational rearrangements of the protein upon ligand occupation, and (iii) ligand−protein interactions. Despite the interest of these data, an accurate interpretation of the electron density in and around the protein binding site is not a straightforward task and it is especially hindered by the relatively low resolution. Furthermore, even in the hypothesis that high-resolution (atomic) structures were available (from 1.0 to 1.5 Å), the inherent complexity of protein structures prevents a straight interpretation of the protein−ligand interactions.[17,18] It is therefore important to remind that the available *structures* remain *models*.

To rationalize and complete these experimental crystallographic observations, several molecular modeling investigations (docking, molecular dynamics) have been used for IMI−AChBP complexes as well as for a series of IMI−nAChR subtypes ($\alpha7$, $\alpha1\beta2$, and $\alpha4\beta2$).[19−23] However, docking and scoring algorithms suffer from intrinsic limitations that often reduce their accuracy.[24,25] In this context, first-principle theoretical studies through hybrid quantum mechanics/molecular mechanics (QM/MM) or multi-quantum chemistry levels (QM/QM′) are known to be useful tools for quantifying both intramolecular and intermolecular interactions that govern protein−ligand binding.[26−29] Indeed, such methods provide accurate molecular geometries, give access to conformational energetics, and are able to delineate the ligand−protein interactions pattern. A QM study using *ab initio* methods (Hartree−Fock (HF) and second-order Moller−Plesset (MP2) levels) has been published on a simplified model considering only the interaction of IMI with nAChR key residues (Arg and Trp).[30] This investigation suggested the importance of both hydrogen bonds (H-bonds) and π-stacking in the binding of IMI to nAChRs. However, an accurate modeling of protein surroundings is still lacking.

In the present work, we use the hybrid (QM/QM′) ONIOM approach within a two-layer scheme[31] to investigate the binding of IMI to *Ac*-AChBP, starting with the available X-ray structure.[16] Previous investigations of imidacloprid structural features have established the flexible character of the ligand in both the crystalline and isolated states.[32−34] In particular, we have recently shown that several conformations of IMI are observed experimentally in the solid state, a feature confirmed by *ab initio* gas phase calculations that allowed us to pinpoint several energetic minima within a 1.2 kcal mol^{-1} range.[34] Therefore, we check here that this behavior in the isolated state pertains to the condensed phase, starting from the experimental structure of IMI bound to AChBP.[15] On the basis of the minimum energy structure obtained, the interactions of IMI with AChBP residues and/or water molecules are quantified through QM/QM′ calculations. To the best of our knowledge, the present work constitutes the first QM/QM′ study of neonicotinoid binding to AChBP. The leading position of IMI in neonicotinoid research (forerunner of this class of insecticides and still the most used worldwide) makes a theoretical investigation aiming at completing the structural data available with energetic parameters highly relevant. By providing accurate structural and energetic properties on several contributions of the AChBP residues involved in the IMI recognition, our work can be used as a basis for the development of novel neonicotinoid ligands targeting specific components of the binding site.

2. COMPUTATIONAL DETAILS

2.1. Definition of the Model System. A crystal structure of IMI bound to *Ac*-AChBP deposited in the Protein Data Bank (PDB code 3C79)[15] was used as a starting point of our study. It is important to recall that AChBP proteins are organized as a pentamer; that is, there are five identical ACh binding sites in each interface where the ligand can be located, though only four out of the five sites are occupied by IMI ligands in the 3C79 crystal structure.[15] Experimental data suggest that these binding sites are equally sensitive to neonicotinoids,[23] and accordingly, the results of theoretical simulations should be independent of the selected binding site. In our case, the active site located in the interface between the B and C subunits has been considered as the starting point to build up the model system. To account for the surroundings of IMI in the *Ac*-AChBP environment, a truncated model was generated, considering all residues with at least one atom interacting with any atom of IMI within an interatomic distance threshold of 4.0 Å. This approach leads to the model represented in Figure 2 composed of one water molecule and 12 amino acids, namely, Tyr55, Tyr93, Val108, Met116, Ile118, Trp147, Val148, Tyr188, Ser189, Cys190, Cys191, and Tyr195. This partition allows us to cover all *Ac*-AChBP residues interacting with IMI and their immediate surroundings.[15] Hydrogen atoms were then

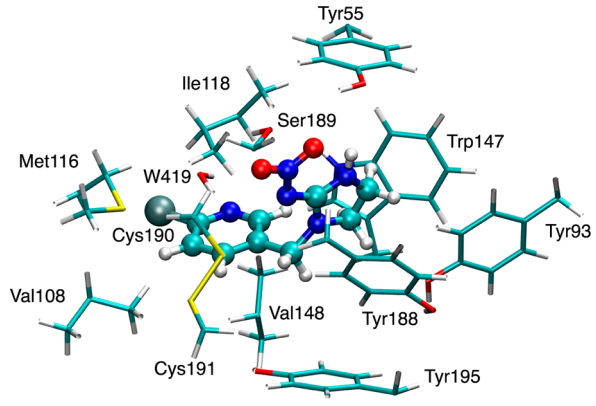

Figure 2. The *Ac*-AChBP−IMI model system considered during the ONIOM calculations. IMI is represented in ball and sticks, while residues are displayed in sticks.

dx.doi.org/10.1021/jp310242n | J. Phys. Chem. B 2013, 117, 3944−3953

added to complete the structure, a step performed with the Pymol program.[35] As usual, in studies of active sites, the N- and C-terminal ends of cut residues were respectively capped with acetyl (CH_3CO-) and N-methyl amino ($-NHCH_3$) groups. The geometries of the capped groups were located in the backbone geometries of the replaced residues.[36,37] The resulting model corresponds to the "real system" (328 atoms) that was investigated with the ONIOM framework.

2.2. ONIOM Calculations. As stated above, experimental studies have pointed out the importance of both H-bonds and π-stacking interactions in the binding of neonicotinoid ligands to nAChRs.[14−16,30] In extended systems, the theoretical treatment of such noncovalent interactions with highly accurate wave function methods, e.g., CCSD(T) or similar,[38,39] is computationally out of reach, and density functional theory (DFT) provides a balanced approach for biological systems. Indeed, huge efforts have been recently devoted to the development of new functionals able to simulate both H-bonds and dispersion, the latter being essential to describe stacking effects.[40,41] For instance, the novel *meta*-hybrid functionals designed by Zhao and Truhlar, and more precisely M06-2X, have been successfully used in the study of noncovalent interactions.[42,43] Unfortunately, the full DFT description of the model shown in Figure 2 remains beyond reach: hybrid QM/QM′ methodologies such as the ONIOM approach,[31] that combines different QM approaches in the same calculation, provide an efficient alternative. In the present contribution, a two-layer ONIOM (QM/QM′) scheme has been adopted as implemented in Gaussian 09.[44] In our approach, the energy for the whole system is computed as

$$E(\mathrm{ONIOM}) = E_{\mathrm{real}}(\mathrm{PM6}) + E_{\mathrm{model}}(\mathrm{M06\text{-}2X/6\text{-}311G(d)}) - E_{\mathrm{model}}(\mathrm{PM6}) \quad (1)$$

where the subscripts indicate the "real system" (containing all atoms) or the "model system" (restricted number of atoms). This combination has been selected because M06-2X provides an excellent description of noncovalent interactions (see above),[46] whereas PM6 is very effective for simulating protein systems, especially when starting from experimental X-ray structures.[47]

The interaction of IMI with AChBP was simulated using two ONIOM schemes. In the first, named ONIOM-1, the QM method was used to describe IMI, and the rest of the system was treated using QM′. The geometry optimizations were carried out within the backbone atoms fixed (BBF) approximation in which the geometries of both IMI and the lateral chains of the amino acids are fully optimized while the atomic positions of the polypeptide chain are frozen.[36,37,48] The minimum nature of the located stationary point was checked through a vibrational calculation (no imaginary frequencies). The geometries of IMI and each single residue in interaction were then extracted in order to compute the pairwise interaction energies, $\Delta E(i, j)$, through the two-body approach,[36]

$$\Delta E(i, j) = E(i, j) - E(i) - E(j) + E_{[\mathrm{BSSE}]} \quad (2)$$

where $E(i, j)$ is the energy of the IMI−residue pair, $E(i)$ and $E(j)$ are the energies of the isolated individual fragments, and $E_{[\mathrm{BSSE}]}$ is the correction for the basis set superposition error (BSSE) computed through the counterpoise method (CP).[49] The *N*-body interaction energies, for larger clusters than a dimer, can be obtained by decomposing the total energy into the constitutive two-body energies.[50,51] Here, a three-body decomposition is used to describe the water bridge in the binding pocket

$$\Delta E(i, j, k) = E(i, j, k) - \Delta E(i, j) - \Delta E(i, k) - \Delta E(j, k) - E(i) - E(j) - E(k) + E_{[\mathrm{BSSE}]} \quad (3)$$

where $E(i, j, k)$ is the total energy of the IMI binding to two residues and $E_{[\mathrm{BSSE}]}$ is the BSSE of the trimer as implemented in the CP method.[49] To check the reliability of the DFT energies, these single-point calculations were computed with both the M06-2X and MP2 approaches. Despite the minor effect of diffuse functions in the computed energies (see the Supporting Information), these single-point calculations have been performed with 6-311++G(d) aiming to provide the most accurate results.

The ONIOM-1 model was subsequently improved by incorporating the residues presenting the strongest interaction energies in the high layer, yielding the ONIOM-2 scheme. The model system was reoptimized within this new ONIOM-2 partition in order to determine accurate interaction energies. Finally, we used the noncovalent interaction (NCI) analysis[52] to gain complementary insights. In the NCI model, the noncovalent interactions are characterized with isosurfaces obtained by combining the computed electron density and its reduced gradient. We refer the reader to a recent paper by Contreras-García and Yang for further methodological details.[53] The NCI analysis has been performed with the NCIPLOT code.[54] Images were rendered using VMD.[55]

3. RESULTS AND DISCUSSION

3.1. Conformational Features of IMI. To ascertain the validity of the M06-2X/6-311G(d) scheme, we have first carried out a conformational analysis of the ligand by computing the potential energy surface (PES) resulting from the rotations around the two single bonds connecting the two rings (see Figure 1). More precisely, starting from the AChBP bound experimental conformation of IMI, we scanned the C9−C5−C4−N3 (D1) and C5−C4−N3−C3 (D2) dihedral angles by steps of 20° between 180 and −180°, all other geometrical parameters being fully optimized (relaxed scan). The resulting PES is displayed in Figure 3, where relative energies are calculated with respect to the global minimum located at D1 and D2 of −94 and 69°, respectively. This minimum indeed corresponds to the IMI-1 structure identified as the most stable conformer in our previous work.[34] Figure 3 also reveals that coplanar rings (dihedrals of ca. 0°, ±180°) correspond to maxima of the PES. Indeed, in IMI, the steric stress between C6 (C9) with N2 (C3) atoms prevents such spatial conformations and induces deviations of both rings from planarity. In addition, the computed PES is consistent with the experimental conformation of the ligand in the *Ac*-AChBP−IMI complex crystal structure: IMI-3C79, D1 = 24° and D2 = 99° is located in a valley.[15] IMI-1 and IMI-3C79 are connected through a very flat surface with an energetic barrier of ca. 5 kcal mol^{-1}; the interconversion between these two conformers is therefore an easy process for the free molecule. This contrasts with the *Ac*-AChBP−IMI complex, where the protein environment constrains the IMI conformation.

3.2. ONIOM-1 Model. *3.2.1. IMI Structural Features.* Let us now move to the structure of IMI−*Ac*-AChBP optimized within the ONIOM-1 model. Selected geometrical parameters

dx.doi.org/10.1021/jp310242n | J. Phys. Chem. B 2013, 117, 3944−3953

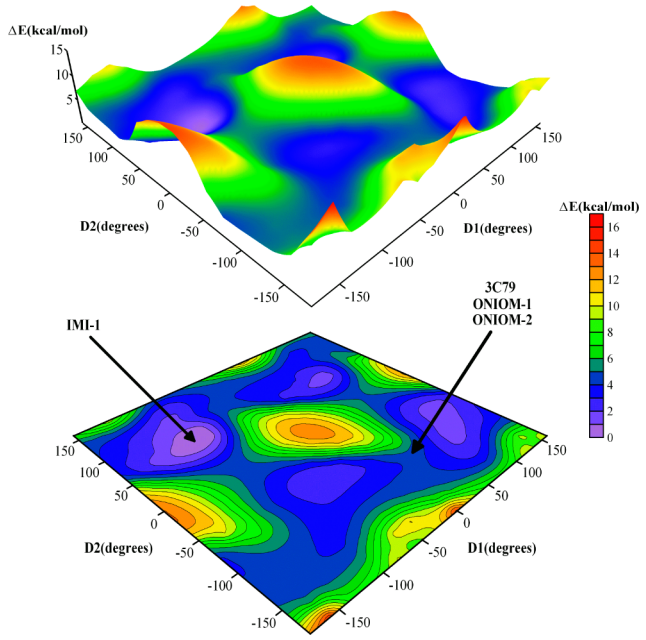

Figure 3. Potential energy surface for simultaneous rotation of the two rings of IMI. Energies are given relatively with respect to the global minimum of free IMI. The arrows indicate the regions of the PES corresponding to the free IMI-1 as well as to the ligand-bound state (IMI-3C79, ONIOM-1, ONIOM-2).

of IMI are listed in Table 1, whereas Figure 4 and Figure S4 (Supporting Information) are superpositions of the IMI

Table 1. Selected Dihedral Angles (in deg) of the IMI Ligand

	D1	D2	D3	D4
3C79[a]	+24.2	−99.3	+1.0	+0.2
ONIOM-1	+39.3	−119.0	+22.8	−18.9
ONIOM-2	+20.2	−98.8	+26.3	−25.0
IMI-1	−94.0	+68.6	+28.5	−23.1

[a]Taken from ref 15.

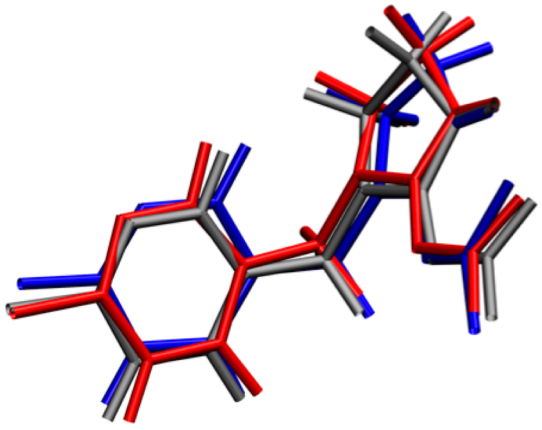

Figure 4. Superposition of the structures of IMI in the *Ac*-AChBP environment: experimental 3C79 structure (blue) as well as ONIOM-1 (red) and ONIOM-2 (gray) geometries.

structure computed at different levels. Compared to the reference crystal structure, the relaxation of the system leads to an increase of dihedrals D1 and D2 by 15 and 20°, respectively, but the relative orientation of both rings remains in the same region of the PES (see Figure 3). Nevertheless, a significant change is observed for the imidazolidine ring: while the five-membered ring adopts a planar conformation in the IMI−*Ac*-AChBP crystal structure (N3−C3−C2−N1: D3 and C3−C2−N1−C1: D4 both close to 0°), the C2 departs from planarity in the optimized ONIOM-1 structure, as illustrated by the variation of D3 and D4 by 23 and −19°, respectively. These angles are also significantly larger than the ones observed in the crystal structure of IMI found in the Cambridge Structural Database (HANFOS) (corresponding D3 and D4 of 7 and −5°, respectively). Indeed, in ONIOM-1, both D3 and D4 are similar to the values predicted for the most stable conformation of free IMI (IMI-1).[34] Consequently, though protein surroundings restrict the relative conformation of the rings by imposing D1 and D2 dihedrals far from the global minimum, IMI presents enough flexibility to relax the imidazolidine ring in the binding pocket.

3.2.2. IMI—Ac-AChBP Complex. As discussed in section 2, we have considered as the starting point the geometry observed in the interface between the B and C subunits. Since the physicochemical properties of IMI are closely related to its nitroimino group, let us start by analyzing the contact of O1 and O2 atoms of IMI with the protein environment (Table 2).

Table 2. Selected Interatomic Distances (in Å) of the IMI *Ac*-AChBP Complex Models[a]

	3C79[b]	ONIOM-1	ONIOM-2
	Nitro Group		
O2−Ser189(OH)	3.41	3.71	3.37
O2−Cys190(N)	2.73	3.00	2.85
O1−Tyr55(OH)	5.06	3.37	2.72
	Water Bridge		
N5−W419(O)	3.02	3.19	2.82
W419(O)−Ile118(N)	3.00	2.87	2.81
W419(O)−Ile118(O)	3.62	4.58	3.07
	Trp147		
C3−Trp147(N)	4.40	3.90	3.77
C3−Trp147(O)	3.00	3.00	2.97
C2−Ce^5(Trp147)	3.98	3.57	3.40
C2−Ce^6(Trp147)	3.40	3.91	3.59
	Other Residues		
Cl−Met116(O)	3.35	2.68	2.75
Ce(IMI)−Ce(Tyr188)	3.89	4.10	4.10

[a]Atoms between brackets indicates the reference site in the residue−ligand distances that have been used to monitor the evolution of the system during the optimization processes. [b]Taken from ref 15.

The O1—Tyr55(OH) H-bond is significantly shorter (1.69 Å) in the ONIOM-1 optimized geometry than in the initial structure. To disclose the origin of such a change, we have compared the O1—Tyr55(OH) distance obtained in our models with the corresponding ones in the other three occupied active sites of the crystal structure. These distances are respectively of 3.2, 3.0, and 2.7 Å in the AB, CD, and DE subunit interfaces: the ONIOM-1 approach restores the O1—Tyr55(OH) H-bond, a trend in agreement with the "average crystal structure" extracted from the four subunit interfaces. Indeed, as discussed by Talley,[15] these experimental data hint that the nitro oxygen atom O1 is engaged in a H-bond with the hydroxyl group of Tyr55. The changes observed in the O2 atom environment are less important, since the theoretical geometry supports its involvement in H-bond contacts with

dx.doi.org/10.1021/jp310242n | J. Phys. Chem. B 2013, 117, 3944−3953

Table 3. Computed Pairwise Interaction Energies (in kcal mol^{-1}) within the ONIOM-1 and ONIOM-2 Schemes[a]

	ONIOM-1			ONIOM-2		
residue	M06-2X	MP2	RMS	M06-2X	MP2	RMS
Tyr55	−4.36	−5.01	1.70	−8.46	−7.65	1.60
Tyr93	−0.39	−0.10	0.31	−3.12	−3.38	0.31
Val108	−2.13	−1.38	0.34	−2.14	−1.20	0.38
Met116	−2.98	−0.56	0.49	−3.55	−1.37	0.48
Ile118	−7.96	−6.88	0.33	−7.61	−6.65	0.27
Trp147	−15.45	−14.37	0.64	−15.44	−14.09	0.60
Val148	−6.96	−6.10	0.31	−7.73	−7.24	0.31
Tyr188	−6.20	−5.92	0.93	−7.13	−5.94	0.99
Ser189	−7.56	−7.34	0.76	−9.26	−8.51	0.76
Cys190−191	−9.54	−7.92	0.48	−11.46	−9.75	0.47
Tyr195	−0.98	−1.70	0.38	−3.36	−3.41	0.46
W419	−1.76	0.25	1.29	−4.15	−2.80	0.50
total	−66.27	−57.04	0.69	−83.43	−72.00	0.66

[a]These calculations were performed at the M06-2X/6-311++G(d) and MP2/6-311++G(d) levels and systematically include CP corrections. For each pair, the RMS deviations (in Å) have been estimated by considering the experimental structure as a reference.

both the OH of Ser189 (3.71 Å) and the backbone NH of Cys190 (3.00 Å). Therefore, our model provides theoretical evidence of the strong H-bond acceptor capacity of the IMI nitro group, consistently with the reported crystal structure data.[34] Additionally, the optimized structure is coherent with the presence of a IMI—W459—Ile118 water bridge through the IMI(N5) and Ile118(N) sites, while the distance between the C3 atom of IMI and the nitrogen atom of the five-membered ring of Trp147 (3.90 Å) as well as the separation between the C2 and the five- and six-membered ring centroids (C2—Ce^5(Trp147) = 3.57 Å and C2—Ce^6(Trp147) = 3.91 Å) suggest that the imidazolidine ring interacts with the Trp indole ring through π-stacking. Along the same lines, the optimized distance between the chlorine atom of IMI and the main chain oxygen of Met116 (2.68 Å) clearly indicates a weak Cl···O═C interaction between the ligand and the polypeptidic chain. Finally, the interval of 4.1 Å between the centroids of the IMI five-membered ring and the aromatic ring of Tyr188 [Ce(IMI)—Ce(Tyr188)] in the ONIOM-1 model is in good agreement with the experimental distance of 3.9 Å. Indeed, contrary to Tyr55, the position of the Tyr188 residue remains constant in the four active sites, with a Ce(IMI)—Ce(Tyr188) distance ranging from 3.9 to 4.1 Å.

In addition, a first NCI analysis was performed on the whole binding pocket using the ONIOM-1 geometry. The main advantage of NCI with respect to other intermolecular analyses is that it offers a direct visualization of noncovalent interactions through colored hypersurfaces computed on the basis of the electronic density gradient. The NCI analysis reveals a complex interaction pattern dominated by weak interactions such as π-stacking (see the Supporting Information). Unfortunately, a purely geometric analysis of such weak interactions is not sufficient to quantify or discriminate the contribution of each single residue in the IMI binding process and further calculations are therefore required to disclose the binding process of the IMI ligand.

3.3. IMI−*Ac*-AChBP Residue Interaction Energies and Refined ONIOM-2 Model. The pairwise interaction energies involved in the IMI−*Ac*-AChBP interactions and the corresponding RMS, computed with respect to the experimental geometry taken as the starting point of the optimization processes, are collated in Table 3. The RMS values shed light on the structural differences between the theoretical and experimental approaches. Total interaction energies are also listed at the bottom of Table 3. The agreement between the M06-2X and MP2 energies is striking, as only W419 presents significant deviations. Indeed, while M06-2X predicts negative interaction energy for this contact, MP2 foresees a slightly positive value. In spite of this dissimilarity, our results confirm the suitability of M06-2X for the description of the IMI−AChBP complex, with a mean absolute error of only ca. 1.00 kcal mol^{-1} and a maximum deviation of 2.42 kcal mol^{-1} with respect to the MP2 values. These deviations can be compared to the ONIOM study of Hannongbua and co-workers[37] of the interaction between galanthamine and acetylcholinesterase. Indeed, in this work, the high layer was treated with the B3LYP functional and the total interaction of the binding pocket was largely overestimated. As these authors demonstrated, this discrepancy is especially large for ligand−amino acid pairs with an important π-stacking component. For instance, the interaction energy computed at the MP2 level for the galanthamine−Trp84 is ca. −4.00 kcal mol^{-1} and becomes positive (ca. 4.00 kcal mol^{-1}) with B3LYP.[37] In the same vein, Wang et al. used HF and MP2 calculations to explore the hydrogen-bonding and cooperative $\pi-\pi$ interactions between IMI and nAChR fragment models.[30] In the case of IMI and Trp fragments, HF and MP2 predicted an interaction of ca. +8.00 and −7.00 kcal mol^{-1}, respectively. Accordingly, binding pockets where π-interactions play a major role, as the IMI−*Ac*-AChBP one, cannot be described at the HF level nor with conventional DFT functionals that are not designed to reproduce dispersion energies.[56,57] In contrast, both M06-2X and MP2 provide similar trends of the IMI interactions which is consistent with the performances of M06-2X for describing weak interactions in biomolecular systems.[42] The comparison of interaction energies can be used to determine the relative contribution of the various residues in the global IMI−*Ac*-AChBP binding. According to Table 3, Trp147 and Cys190−191 are the most important contributors to the total interaction energy, with respective M06-2X (MP2) values of −15.45 (−14.37) and −9.54 (−7.92) kcal mol^{-1}. This represents ca. 40% of the total interaction energy.

To improve both the simulated geometries and interaction energies, we have then incorporated these two Trp147 and Cys190−191 residues in the high layer. In addition, since both the crystal structure and the ONIOM-1 geometry indicate that

the N5 pyridinic nitrogen of IMI is hydrogen-bonded to the W419 water molecule, itself bridged to Ile118, while the nitro group interacts with Ser189 O,[23] we have also included these three residues in the high layer, leading to the ONIOM-2 model. The results obtained are summarized in Tables 1−3 and in Figures 4 and 5. Table 1 shows that the relative orientation

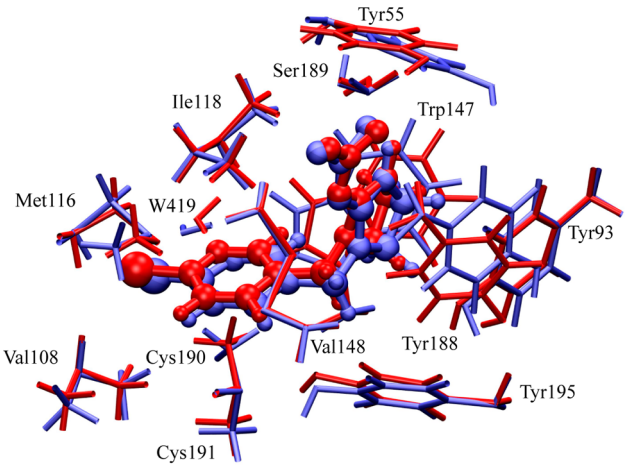

Figure 5. Overlays of the experimental (3C79 PDB entry, blue) and theoretical (ONIOM-2, red) IMI−*Ac*-AChBP structures.

of the two rings matches the data of the 3C79 crystal structure, while D3 and D4 angles coincide with the values obtained in the global minimum IMI-1 at the M06-2X/6-311G(d) level (differences <4°). This confirms the restriction imposed by the protein surroundings on the orientation between the two rings as well as the out-of-planarity disposition of C2 in the five-membered ring (see Figure 4). The interatomic distances listed in Table 2 show that the H-bonds involved in the water bridge are predicted to be stronger with the ONIOM-2 model than with the simpler ONIOM-1 approach, with the distances of the three interactions being significantly shortened. Additionally, Figure 5 indicates that the amino acids vicinal to the IMI nitro group (Tyr55 and Ser189) orientate their hydroxyl groups toward the O2 and O1 atoms in agreement with shortening of the O1−Tyr55(OH) and O2−Ser189(OH) distances. We emphasize that other residues are significantly reoriented in order to optimize the different interactions, i.e., to bring their functional groups closer to the IMI ligand. This is particularly noticeable for the interaction with the hydroxyl of Tyr195, that did not appear as a close contact in 3C79 nor in ONIOM-1. These structural alterations are more easily assessed through the RMS collected in Table 3. The most significant changes between the ONIOM models and the experimental structure are observed for Tyr55 (1.6−1.7 Å) and Tyr188 (0.9−1.0 Å). As indicated previously, the large shift observed for Tyr55 through our ONIOM models is explained by the fact that the geometry optimizations favor a H-bond between the OH group of Tyr55 and one nitro oxygen of IMI. This interaction is observed in three out of the four binding interfaces of AChBP occupied by IMI in the crystal structure.[15] The alteration observed for Tyr188 has to be put in perspective owing to the similar distances measured in the experimental geometries between the centroids of the IMI five-membered ring and the Tyr 188 aromatic ring, Ce(IMI)−Ce(Tyr188) (average of 4.00 Å), and the ones obtained after the geometry optimization with the ONIOM-1 and ONIOM-2 models (4.10 Å). Lastly, the large shift of the water molecule (1.3 and 0.5 Å with the ONIOM-1 and ONIOM-2 methodologies) is explained by a maximization of the H-bond interactions that it relays between the AChBP Ile118 residue and IMI.

We have also analyzed the interplay between the structural changes and the corresponding interaction energies. According to Table 3, the relaxation of the IMI−*Ac*-AChBP model yields more negative interaction energies of Tyr55, Ser189, Cys190−191, and W419 at ONIOM-2 than at the ONIOM-1 level. Indeed, the total interaction energy is ca. 15 kcal mol^{-1} more negative with ONIOM-2 than with the simpler model. We emphasize that the impact in binding mode is not uniform, e.g., the interaction energy with Ile118 and Trp147 remains unaltered by the increase of the high layer region, whereas the interaction IMI−Tyr55 is significantly increased in ONIOM-2. The larger negative energy is the logical consequence of the geometric changes depicted in Table 2. Despite these differences, Trp147 and Cys190−191 remain the key residues (larger interaction energies) of the IMI−AChBP binding site within the ONIOM-2 model.

3.4. NCI Analysis. A NCI analysis[50−52] has been carried out considering for the key residues indicated by the ONIOM-2 calculations (Trp147, Cys190−191, Ile118, and Tyr188) in interaction with IMI. Although the two latter residues appear ranked in fifth and seventh positions according to our interaction energy scale, mutagenesis experiments have hinted their great importance in the neonicotinoid binding mode.[58] The interaction with the Tyr55 residue has also been investigated to identify the H-bond with the nitro group of the IMI. As shown in Figures S1 and S2 (Supporting Information), the IMI−*Ac*-AChBP complex model is dominated by weak interactions. Since the visualization of all interactions in large systems leads to quite complex pictures, the NCI analysis was performed for the selected IMI−residue pairs rather than on the whole IMI−*Ac*-AChBP model system. Accordingly, gradient isosurfaces for IMI−Tyr55, IMI−Ile118, IMI−Trp147, IMI−Tyr188, and IMI−Cys190−191 as well as the water bridge IMI−W459−Ile118 are displayed in Figure 6. In agreement with the O2···Cys190(N) distance reported in Table 2 (2.85 Å), the O2 atom of the nitro group of IMI is H-bonded with the NH backbone atom of Cys190. Secondary contacts between the methylene groups of IMI and the sulfur atoms of the disulfide Cys190−191 bridge and between methylene groups of Cys 190−191 and the imino nitrogen of IMI are also suggested by the NCI analysis. The H-bond confirmed in the NCI analysis provides theoretical support for the directionality of the O2 atom toward the Cys190 NH backbone observed experimentally.[23] Accordingly, the importance of the Cys190−191 dipeptide in the global ligand−protein interaction can be attributed both to H-bonds and multiple van der Waals contacts. In order to estimate the relative contributions of the Cys190−191 S atoms and the NH of the polypeptide chain in the IMI−AChBP interaction, we performed a calculation in which the backbone components have been removed from the original pair. The van der Waals contacts are estimated to contribute to the interaction by −6.53 kcal mol^{-1}. The difference with the total energy of −11.63 kcal mol^{-1} (Table 3), of ca. −5 kcal mol^{-1}, is consistent with the expected value for an ordinary H-bond.[57] NCI also identifies the O1−Tyr55(OH) interaction as a H-bond, suggesting that the directionality of the nitro group is not only due to the interaction with Cys190(N) but also partially governed by the Tyr55 residue located in the complementary face. Figure 6

dx.doi.org/10.1021/jp310242n | J. Phys. Chem. B 2013, 117, 3944−3953

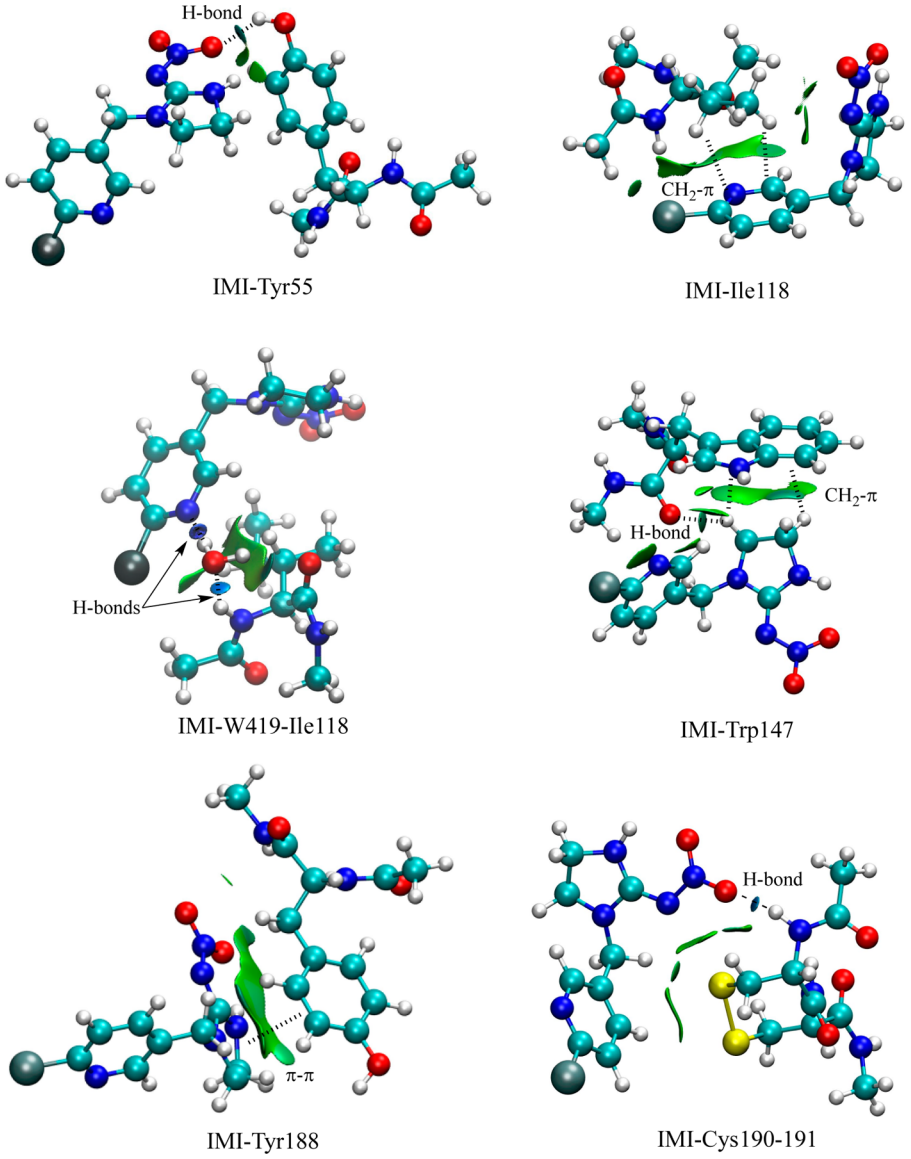

Figure 6. NCI analysis of selected IMI−residue pairs. Isosurfaces correspond to s = 0.3 au with a color scale of −0.045 au < ρ < 0.045 au, using promolecular densities. H-bonds are displayed in blue, and weak interactions are represented in green.

shows that the IMI−Trp147 interaction mainly involves CH···π bonds between the imidazolidine CH_2−CH_2 moiety of IMI and the aromatic system of Trp147. Consequently, the distances between the IMI C2 and C3 carbon atoms and the centroids of the five- and six-membered rings of Trp147 are, respectively, of 3.40 and 3.59 Å, whereas the distances measured with respect to the closest linked C2 and C3 H atoms are 3.00 and 2.73 Å, respectively. These values are at the borderline between stacked and H-bond arrangements. However, the distance between the C3 IMI atom and the carbonyl oxygen atom, of 2.97 Å, leads to values of 2.29 and 2.88 Å when the C3 H atoms are considered. This interaction can be seen as a weak H-bond involved in the IMI binding. In short, the NCI analysis demonstrates that several CH···π interactions together with a weak CH···O H-bond explain the large interaction of IMI in the AChBP binding pocket.

The NCI analysis points out that the IMI−Ile118 interaction involves secondary contacts between CH groups of the Ile118 lateral chain and the π-system of the IMI pyridine ring. These latter interactions significantly contribute to the final interaction energy of −7.46 kcal mol^{-1} (Table 2). Since the N5 pyridinic nitrogen of IMI has been proposed to form a H-bond with the backbone carbonyl via a water bridge,[23] we complete the analysis of Ile118 by computing the interaction energy of the trimer IMI−W459−Ile118. According to eq 3, the predicted energy for this trimer is −22.42 kcal mol^{-1}, 14.81 kcal mol^{-1} more stable than the IMI−Ile118 pair. This significant difference highlights the importance of the two strong H-bonds (blue isosurfaces in Figure 6) involved in the water molecule bridge in the IMI binding mode. The computed isosurface for the IMI−Tyr188 pair clearly indicates the π−π stacking nature of the interaction between the five-membered ring of IMI and the aromatic side chain of Tyr188. Since such interactions are known to tune IMI's activity,[60] our results show the interest of the present methodology for a comprehensive understanding of neonicotinoid−AChBP interactions.

The NCI analysis reveals that IMI interacts with the Met116 residue through an interaction larger than typical van der Waals effects but smaller than the IMI−W419 and IMI−Cys190−191 H-bonds (Figure 7 and Figure S1, Supporting Information). As

dx.doi.org/10.1021/jp310242n | J. Phys. Chem. B 2013, 117, 3944−3953

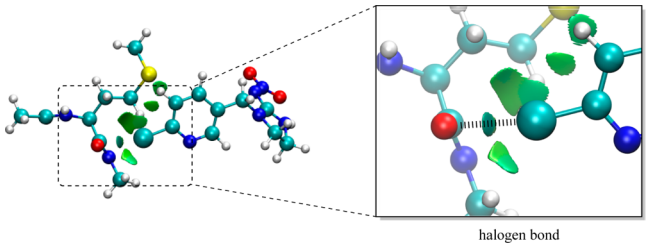

Figure 7. NCI analysis of IMI−Met116. The isosurface corresponds to s = 0.3 au and a color scale of −0.045 au < ρ < 0.045 au. The predicted halogen-bond distance in the ONIOM-2 model is 2.75 Å.

expected from the geometrical data listed in Table 2, NCI confirms the contribution of a halogen-bond interaction in the IMI−*Ac*-AChBP binding process. Indeed, as recently proposed by Duan and co-workers,[61] the interaction between the Cl atom of IMI and the O atom of the Met116 residue can be attributed to a halogen bond. Halogen bonds[62] with Cl in biomolecules are defined as short C−Cl···O−Y interactions, the distance being smaller or equal to the sum of their van der Waals radii (3.27 Å).[63] Both the value of the optimized Cl−Met116(O) distance (2.75 Å) and the predicted density surface (Figure 7) are consistent with the presence of such Cl···O halogen bond.

CONCLUSIONS

The binding of IMI to *Ac*-AChBP has been investigated using two-layer ONIOM models (M06-2X/6-311G(d):PM6) in order to discriminate, rationalize, and quantify the contribution of the key residues of the protein binding site. First, only IMI has been located in the high layer, while the rest of the protein is included in the low layer (ONIOM-1). Within this partition scheme, the flexibility of the IMI ligand has been confirmed, with significant modifications of inter-ring dihedrals being observed in the protein surroundings. The subsequent DFT and post-HF calculations of IMI−AChBP pairwise interactions have been used to decompose the binding energy. In a second step, the main contributors to the interaction energy revealed from this analysis have been included in a more complex ONIOM-2 model. Using this second partition scheme, the contribution of the different *Ac*-AChBP residues have been delineated. The main contributors to the binding energy are Trp147 (−15.38 kcal mol^{-1}) and Cys190−191 (−11.63 kcal mol^{-1}) residues, and they account for ca. 40% of the total interaction energy. While the IMI−Trp147 interaction can only be explained by several weak CH···π interactions, the interaction energy of the IMI−Cys190−191 pair can be rationalized in terms, on the one hand, of van der Waals contacts between CH groups of IMI and the sulfur atoms of the AChBP residues and, on the other hand, of a H-bond interaction between the nitro group of IMI and the main chain NH of Cys190. Furthermore, an additional interaction between the OH group of Tyr195 and the IMI ligand has been unravelled. Finally, significant variation of the structural parameters of the IMI−AChBP is predicted for the Tyr55 group. Indeed, this residue exhibits the largest deviation from the experimental X-ray structure (RMS of 1.70 and 1.60 Å for the ONIOM-1 and ONIOM-2 models, respectively). However, the global RMS value (<0.70 Å) hints that our model system reproduces the most important interactions in the binding pocket.

A NCI analysis on selected IMI−AChBP residue pairs has allowed some complementary insights. In particular, the key role of Trp147 in the IMI binding is rationalized thanks to the existence of several weak CH···π contacts involving CH groups and unsaturated fragments of both entities. The pivotal contribution of the Cys190−191 dipeptide is explained through the presence of both H-bond interactions between an oxygen atom of the IMI nitro group and the NH main chain group of Cys190, and weak van der Waals contacts between the Cys190−191 sulfur atoms and IMI CH groups. The contributions of other key residues suggested through mutagenesis experiments, namely, Ile118 and Tyr188, are rationalized through CH···π (IMI) and π···π contacts, respectively. Furthermore, the contribution of a halogen bond involving the chlorine atom of IMI and the main chain carbonyl group of Met116 is suggested by our computations.

On the whole, the approach presented in this work provides a detailed description (geometry, type of interaction, relative contribution to the binding energy) of the key interactions occurring in the IMI binding to AChBP. Consequently, it offers new perspectives for the development of novel neonicotinoid ligands targeting specific components of the binding site.

ASSOCIATED CONTENT

Supporting Information

(1) NCI analysis for the whole IMI−*Ac*-AChBP model system in the ONIOM-1 (movie) and ONIOM-2 (figures) geometries; (2) optimized IMI-1 and IMI−ONIOM-2 geometries; (3) interaction energies computed at the M06-2X/6-311G(d) and MP2/6-311G(d) levels; (4) Cartesian coordinates of the ONIOM-1 and ONIOM-2 optimized geometries; (5) complete ref 44. This material is available free of charge via the Internet at http://pubs.acs.org.

AUTHOR INFORMATION

Corresponding Author

*Phone: 33 (0)2 51 12 55 63. Fax: 33 (0)2 51 12 54 02. E-mail: Jose.Ceron@univ-nantes.fr (J.P.C.-C.); Jean-Yves.Le-Questel@univ-nantes.fr (J.-Y.L.Q.).

Notes

The authors declare no competing financial interest.

ACKNOWLEDGMENTS

The authors thank the two anonymous referees for suggestions that substantially improved the paper. J.P.C.-C. acknowledges the fellowship provided by the Fundación Séneca, Agencia de Ciencia y Tecnología de la Región de Murcia, within its Postdoctoral Research Staff Training Program. D.J. acknowledges the European Research Council (ERC) and the *Région des Pays de la Loire* for financial support in the framework of Starting Grant (Marches - 278845) and a *recrutement sur poste stratégique*, respectively. This work was granted access to the HPC resources of [CCRT/CINES/IDRIS] under the allocation c2012085117 made by GENCI (Grand Equipement National de Calcul Intensif). The authors gratefully acknowledge the CCIPL (Centre de Calcul Intensif des Pays de la Loire) for grants of computer time.

REFERENCES

(1) Corringer, P. J.; Le Novere, N.; Changeux, J. P. Nicotinic Receptors at the Amino Acid Level. *Annu. Rev. Pharmacol. Toxicol.* **2000**, *40*, 431−458.

(2) Karlin, A. Emerging Structure of the Nicotinic Acetylcholine Receptors. *Nat. Rev. Neurosci.* **2002**, *3*, 102−114.

(3) Grutter, T.; Changeux, J. P. Nicotinic Receptors in Wonderland. *Trends Biochem. Sci.* **2001**, *26*, 459−463.
(4) Matsuda, K.; Buckingham, S. D.; Kleier, D.; Rauh, J. J.; Grauso, M.; Sattelle, D. B. Neonicotinoids: Insecticides Acting on Insect Nicotinic Acetylcholine Receptors. *Trends Pharmacol. Sci.* **2001**, *22*, 573−580.
(5) Matsuda, K.; Shimomura, M.; Ihara, M.; Akamatsu, M.; Sattelle, D. B. Neonicotinoids Show Selective and Diverse Actions on Their Nicotinic Receptor Targets: Electrophysiology, Molecular Biology, and Receptor Modeling Studies. *Biosci. Biotechnol. Biochem.* **2005**, *69*, 1442−1452.
(6) Tomizawa, M.; Casida, J. E. Selective Toxicity of Neonicotinoids Attributable to Specificity of Insect and Mammalian Nicotinic Receptors. *Annu. Rev. Entomol.* **2003**, *48*, 339−364.
(7) Jeschke, P.; Nauen, R. Neonicotinoids: From Zero to Hero in Insecticide Chemistry. *Pest. Manag. Sci.* **2008**, *64*, 1084−1098.
(8) Jeschke, P.; Nauen, R.; Schindler, M.; Elbert, A. Overview of the Status and Global Strategy for Neonicotinoids. *J. Agric. Food Chem.* **2011**, *59*, 2897−2908.
(9) Kagabu, S. Discovery of Imidacloprid and Further Developments from Strategic Molecular Designs. *J. Agric. Food Chem.* **2011**, *59*, 2887−2896.
(10) Wells, G. B. Structural Answers and Persistent Questions about How Nicotinic Receptors Work. *Front. Biosci.* **2008**, *13*, 5479−5510.
(11) Liu, Z. W.; Williamson, M. S.; Lansdell, S. J.; Denholm, I.; Han, Z. J.; Millar, N. S. A Nicotinic Acetylcholine Receptor Mutation Conferring Target-Site Resistance to Imidacloprid in Nilaparvata Lugens (Brown Planthopper). *Proc. Natl. Acad. Sci. U.S.A.* **2005**, *102*, 8420−8425.
(12) Liu, Z.; Han, Z.; Zhang, Y.; Song, F.; Yao, X.; Liu, S.; Gu, J.; Millar, N. S. Heteromeric Co-assembly of Two Insect Nicotinic Acetylcholine Receptor Alpha Subunits: Influence on Sensitivity to Neonicotinoid Insecticides. *J. Neurochem.* **2009**, *108*, 498−506.
(13) Liu, Z.; Han, Z.; Liu, S.; Zhang, Y.; Song, F.; Yao, X.; Gu, J. Amino Acids Outside of the Loops that Define the Agonist Binding Site Are Important for Ligand Binding to Insect Nicotinic Acetylcholine Receptors. *J. Neurochem.* **2008**, *106*, 224−230.
(14) Tomizawa, M.; Casida, J. E. Molecular Recognition of Neonicotinoid Insecticides: The Determinants of Life or Death. *Acc. Chem. Res.* **2009**, *42*, 260−269.
(15) Talley, T. T.; Harel, M.; Hibbs, R. E.; Radic, Z.; Tomizawa, M.; Casida, J. E.; Taylor, P. Atomic Interactions of Neonicotinoid Agonists with AChBP: Molecular Recognition of the Distinctive Electronegative Pharmacophore. *Proc. Natl. Acad. Sci. U.S.A.* **2008**, *105*, 7606−7611.
(16) Ihara, M.; Okajima, T.; Yamashita, A.; Oda, T.; Hirata, K.; Nishiwaki, H.; Morimoto, T.; Akamatsu, M.; Ashikawa, Y.; Kuroda, S.; Mega, R.; Kuramitsu, S.; Sattelle, D. B.; Matsuda, K. Crystal Structures of Lymnaea Stagnalis AChBP in Complex with Neonicotinoid Insecticides Imidacloprid and Clothianidin. *Invertebr. Neurosci.* **2008**, *8*, 71−81.
(17) Davis, A. M.; St-Gallay, S. A.; Kleywegt, G. J. Limitations and Lessons in the Use of X-ray Structural Information in Drug Design. *Drug Discovery Today* **2008**, *13*, 831−841.
(18) Liebeschuetz, J.; Hennemann, J.; Olsson, T.; Groom, C. R. The Good, the Bad and the Twisted: A Survey of Ligand Geometry in Protein Crystal Structures. *J. Comput.-Aided Mol. Des.* **2012**, *26*, 169−183.
(19) Taly, A.; Colas, C.; Malliavin, T.; Blondel, A.; Nilges, M.; Corringer, P.-J.; Joseph, D. Discrimination of Agonists versus Antagonists of Nicotinic Ligands Based on Docking onto AChBP Structures. *J. Mol. Graphics Modell.* **2011**, *30*, 100−109.
(20) Liu, G.-Y.; Ju, X.-L.; Cheng, J. Selectivity of Imidacloprid for Fruit Fly versus Rat Nicotinic Acetylcholine Receptors by Molecular Modeling. *J. Mol. Model.* **2010**, *16*, 993−1002.
(21) Amiri, S.; Shimomura, M.; Vijayan, R.; Nishiwaki, H.; Akamatsu, M.; Matsuda, K.; Jones, A. K.; Sansom, M. S. P.; Biggin, P. C.; Sattelle, D. B. A Role for Leu118 of Loop E in Agonist Binding to the α7 Nicotinic Acetylcholine Receptor. *Mol. Pharmacol.* **2008**, *73*, 1659−1667.
(22) Rocher, A.; Marchand-Geneste, N. Homology Modelling of the Apis Mellifera Nicotinic Acetylcholine Receptor (nAChR) and Docking of Imidacloprid and Fipronil Insecticides and Their Metabolites. *SAR QSAR Environ. Res.* **2008**, *19*, 245−261.
(23) Tomizawa, M.; Talley, T. T.; Maltby, D.; Durkins, K. A.; Medzihradszky, K. F.; Burlingame, A. L.; Taylor, P.; Casida, J. E. Mapping the Elusive Neonicotinoid Binding Site. *Proc. Natl. Acad. Sci. U.S.A.* **2007**, *104*, 9075−9080.
(24) Li, X.; Li, Y.; Cheng, T. J.; Liu, Z. H.; Wang, R. X. Evaluation of the Performance of Four Molecular Docking Programs on a Diverse Set of Protein-Ligand Complexes. *J. Comput. Chem.* **2010**, *31*, 2109−2125.
(25) Cross, J. B.; Thompson, D. C.; Rai, B. K.; Baber, J. C.; Fan, K. Y.; Hu, Y. B.; Humblet, C. Comparison of Several Molecular Docking Programs: Pose Prediction and Virtual Screening Accuracy. *J. Chem. Inf. Model.* **2009**, *49*, 1455−1474.
(26) Guallar, V.; Wallrapp, F. H. QM/MM Methods: Looking Inside Heme Proteins Biochemistry. *Biophys. Chem.* **2010**, *149*, 1−11.
(27) De Vivo, M. Bridging Quantum Mechanics and Structure-Based Drug Design. *Front. Biosci.* **2011**, *16*, 1619−1633.
(28) Menikarachchi, L. C.; Gascón, J. A. QM/MM Approaches in Medicinal Chemistry Research. *Curr. Top. Med. Chem.* **2010**, *10*, 46−54.
(29) Senn, H. M.; Thiel, W. QM/MM Methods for Biomolecular Systems. *Angew. Chem., Int. Ed. Engl.* **2009**, *48*, 1198−1229.
(30) Wang, Y.; Cheng, J.; Qian, X.; Li, Z. Actions between Neonicotinoids and Key Residues of Insect nAChR Based on an Ab Initio Quantum Chemistry Study: Hydrogen Bonding and Cooperative π−π Interaction. *Bioorg. Med. Chem.* **2007**, *15*, 2624−2630.
(31) Vreven, T.; Byun, K. S.; Komaromi, I.; Dapprich, S.; Montgomery, J. A., Jr.; Morokuma, K.; Frisch, M. J. Combining Quantum Mechanics Methods with Molecular Mechanics Methods in ONIOM. *J. Chem. Theory Comput.* **2006**, *2*, 815−826.
(32) Kagabu, S.; Matsuno, H. Chloronicotinyl Insecticides. 8. Crystal and Molecular Structures of Imidacloprid and Analogous Compounds. *J. Agric. Food Chem.* **1997**, *45*, 276−281.
(33) Chopra, D.; Mohan, T. P.; Rao, K. S.; Row, T. N. G. (2*E*)-1-[(6-Chloropyridin-3-yl)methyl]-*N*-nitroimidazolidin-2-imine (Imidachloprid). *Acta Crystallogr.* **2004**, *E60*, O2415−O2417.
(34) Le Questel, J.-Y.; Graton, J.; Cerón-Carrasco, J. P.; Jacquemin, D.; Planchat, A.; Thany, S. H. New Insights on the Molecular Features and Electrophysiological Properties of Dinotefuran, Imidacloprid and Acetamiprid Neonicotinoid Insecticides. *Bioorg. Med. Chem.* **2011**, *19*, 7623−7634.
(35) Delano, W. L. *The Pymol Molecular Graphics System*; Delano Scientific: San Carlos, CA, 2004 (http://www.pymol.org).
(36) Saen-oon, S.; Kuno, M.; Hannongbua, S. Binding Energy Analysis for Wild-Type and Y181C Mutant HIV-1 RT/8-Cl*TIBO* Complex Structures: Quantum Chemical Calculations Based on the ONIOM Method. *Proteins: Struct., Funct., Bioinf.* **2005**, *61*, 859−869.
(37) Kitisripanya, N.; Saparpakorn, P.; Wolschann, P.; Hannongbua, S. Binding of Huperzine A and Galanthamine to Acetylcholinesterase, Based on ONIOM Method. *Nanomed-Nanotechnol. Biol. Med.* **2011**, *7*, 60−68.
(38) Sponer, J.; Riley, K. E.; Hobza, P. Nature and Magnitude of Aromatic Stacking of Nucleic Acid Bases. *Phys. Chem. Chem. Phys.* **2008**, *10*, 2595−2610.
(39) Hobza, P.; Sponer, J. Toward True DNA Base-Stacking Energies: MP2, CCSD(T), and Complete Basis Set Calculations. *J. Am. Chem. Soc.* **2002**, *124*, 11802−11808.
(40) Zhao, Y.; Truhlar, D. G. Hybrid Meta Density Functional Theory Methods for Thermochemistry, Thermochemical Kinetics, and Noncovalent Interactions: The MPW1B95 and MPWB1K Models and Comparative Assessments for Hydrogen Bonding and van der Waals Interactions. *J. Phys. Chem. A* **2004**, *108*, 6908−6918.
(41) Zhao, Y.; Truhlar, D. G. How Well Can New-Generation Density Functional Methods Describe Stacking Interactions in Biological Systems? *Phys. Chem. Chem. Phys.* **2005**, *7*, 2701−2705.

(42) Zhao, Y.; Schultz, N. E.; Truhlar, D. G. Density Functionals with Broad Applicability in Chemistry. *Acc. Chem. Res.* **2008**, *41*, 157−167.
(43) Zhao, Y.; Truhlar, D. G. The M06 Suite of Density Functionals for Main Group Thermochemistry, Thermochemical Kinetics, Noncovalent Interactions, Excited States, and Transition Elements: Two New Functionals and Systematic Testing of Four M06-Class Functionals and 12 Other Functionals. *Theor. Chem. Acc.* **2008**, *120*, 215−241.
(44) Frisch, M. J.; Trucks, G. W.; Schlegel, H. B.; Scuseria, G. E.; Robb, M. A.; Cheeseman, J. R.; Scalmani, G.; Barone, V.; Mennucci, B.; Petersson, G. A.; et al. *Gaussian 09*, revision A.02; Gaussian, Inc.: Wallingford, CT, 2009.
(45) Stewart, J. J. P. Optimization of Parameters for Semiempirical Methods V: Modification of NDDO Approximations and Application to 70 Elements. *J. Mol. Model.* **2007**, *13*, 1173−1213.
(46) Rutledge, L. R.; Wetmore, S. D. Modeling the Chemical Step Utilized by Human Alkyladenine DNA Glycosylase: A Concerted Mechanism Aids in Selectively Excising Damaged Purines. *J. Am. Chem. Soc.* **2011**, *133*, 16258−16269.
(47) Stewart, J. J. P. Application of the PM6 Method to Modeling Proteins. *J. Mol. Model.* **2009**, *15*, 765−805.
(48) Boonsri, P.; Kuno, M.; Hannongbua, S. Key Interactions of the Mutant HIV-1 Reverse Transcriptase/efavirenz: An Evidence Obtained from ONIOM Method. *Med. Chem. Commun.* **2011**, *2*, 1181−1187.
(49) Boys, S.; Bernardi, F. The Calculations of Small Molecular Interaction by the Difference of Separate Total Energies. Some Procedures with Reduced Error. *Mol. Phys.* **1970**, *19*, 553−566.
(50) Hankins, D.; Moskowitz, J. W. Water Molecule Interactions. *J. Chem. Phys.* **1970**, *53*, 4544−4554.
(51) Dziekonski, P.; Sokalski, W. A.; Leszczynski, J. Physical Nature of Environmental Effects on Intermolecular Proton Transfer in (O2NOH···NH3)(H2O)n and (ClH···NH3)(H2O)n (n=1−3) Complexes. *Chem. Phys.* **2001**, *272*, 37−45.
(52) Johnson, E. R.; Keinan, S.; Mori-Sánchez, P.; Contreras-García, J.; Cohen, A. J.; Yang, W. Revealing Noncovalent Interactions. *J. Am. Chem. Soc.* **2010**, *132*, 6498−6506.
(53) Contreras-García, J.; Yang, W.; Johnson, E. R. Analysis of Hydrogen-Bond Interaction Potentials from the Electron Density: Integration of Noncovalent Interaction Regions. *J. Phys. Chem. A* **2011**, *115*, 12983−12990.
(54) Contreras-García, J.; Johnson, E. R.; Keinan, S.; Chaudret, R.; Piquemal, J.-P.; Beratan, D. N.; Yang, W. NCIPLOT: A Program for Plotting Noncovalent Interaction Regions. *J. Chem. Theory Comput.* **2001**, *7*, 625−632.
(55) Humphrey, W.; Dalke, A.; Schulten, K. VMD: Visual Molecular Dynamics. *J. Mol. Graphics* **1996**, *14*, 33−38.
(56) Sousa, S. F.; Fernandes, P. A.; Ramos, M. J. General Performance of Density Functionals. *J. Phys. Chem. A* **2007**, *111*, 10439−10452.
(57) van der Wijst, T.; Fonseca-Guerra, C.; Swart, M.; Bickelhaupt, F. Performance of Various Density Functionals for the Hydrogen Bonds in DNA Base Pairs. *Chem. Phys. Lett.* **2006**, *426*, 415−421.
(58) Matsuda, K.; Kanaoka, S.; Akamatsu, M.; Sattelle, D. B. Diverse Actions and Target-Site Selectivity of Neonicotinoids: Structural Insights. *Mol. Pharmacol.* **2009**, *76*, 1−10.
(59) Perrin, C. L.; Nielson, J. B. "Strong" Hydrogen Bonds in Chemistry and Biology. *Annu. Rev. Phys. Chem.* **1997**, *48*, 511−544.
(60) Zhang, W.; Yang, X.; Chen, W.; Xu, X.; Li, L.; Zhai, H.; Zhong, L. Design, Multicomponent Synthesis, and Bioactivities of Novel Neonicotinoid Analogues with 1,4-Dihydropyridine Scaffold. *J. Agric. Food Chem.* **2010**, *58*, 2741−2745.
(61) Duan, H.; Zhang, W.; Zhao, J.; Liang, D.; Yang, X.; Jin, S. A Novel Halogen Bond and a Better-known Hydrogen Bond Cooperation of Neonicotinoid and Insect Nicotinic Acetylcholine Receptor Recognition. *J. Mol. Model.* **2012**, *18*, 3867−3875.
(62) Metrangolo, P.; Resnati, G. Halogen Bonding: A Paradigm in Supramolecular Chemistry. *Chem.—Eur. J.* **2001**, *7*, 2511−2519.
(63) Parisini, E.; Metrangolo, P.; Pilati, T.; Resnati, G.; Terraneo, G. Halogen Bonding in Halocarbon-Protein Complexes: A Structural Survey. *Chem. Soc. Rev.* **2011**, *40*, 2267−2278.